

MESH GENERATION FOR hp TYPE FINITE ELEMENT ANALYSIS OF REISSNER-MINDLIN PLATES

STEFAN M. HOLZER

*Informationsverarbeitung im Konstruktiven Ingenieurbau, Universität Stuttgart, Pfaffenwaldring 7, D-70550 Stuttgart,
Germany*

ABSTRACT

Efficient finite element (FE) analyses of Reissner-Mindlin (RM) plate bending problems require a combination of high-order polynomial trial functions (p -extension) and locally refined meshes, or, in short, an hp -extension of the FE method. In the optimal case, exponential rates in the convergence of the error in energy norm can be obtained by such a discretization. This contribution discusses strategies for the *fully automatic* generation of finite element meshes that fulfill all the *a priori* requirements on mesh design for hp -type approximations of RM plate bending problems on general domains. At the same time, the resulting meshes are required to be "as coarse as possible" and consists purely of quadrilaterals. Numerical examples show that the meshes generated by our approach are indeed suitable for achieving very fast convergence on practical examples. Also, we present numerical investigations on the effects of mesh design on convergence in the presence of boundary layer effects, point singularities, and both combined.

key words: mesh generation, coarse meshing, hp finite elements, Reissner-Mindlin plate theory, boundary layer effect.

1. INTRODUCTION

RM plate bending problems are among the most important and at the same time most thoroughly studied problems of practical engineering relevance. Nevertheless, finite element tools which exploit all the known features of the solution by fully automatic, specifically tailored "optimal" discretizations are not yet available. It is the goal of the present study to demonstrate that fully automatic mesh design, starting from *a priori* data, is feasible even for general, complicated geometries such as are usually given by practical applications, and to add ample numerical, experimental evidence showing the efficiency, reliability and robustness of an approach based on hp -extension.

We consider a domain $\Omega \subset \mathfrak{R}^2$ occupied by an isotropic, homogeneous plate of thickness t subject to a load $q(x, y)$. We denote by w the transverse displacement and by $\vec{\beta}$ the rotations of the plate. The plate bending problem is governed by the following set of equilibrium equations:

$$-\frac{D}{2}[(1-\nu)\Delta\vec{\beta} + (1+\nu)\nabla\nabla\cdot\vec{\beta}] - \kappa Gt(\nabla w - \vec{\beta}) = 0 \quad (1)$$

$$\kappa Gt\nabla\cdot(\nabla w - \vec{\beta}) = q \quad (2)$$

Here, $D = \frac{Et^3}{12(1-\nu^2)}$ is the bending constant, E is Young's modulus, $G = \frac{E}{2(1+\nu)}$ is the shear modulus, κ the shear correction factor (taken to be $\kappa = \frac{5}{6}$ throughout the rest of this contribution). We consider the following types of boundary conditions: Soft simple support ($w = 0$) and hard clamped support ($w = 0, \vec{\beta} = 0$). Furthermore, we consider unsupported free edges.

The variational form of (1), (2) reads: Find $u = (w, \vec{\beta}) \in H$ such that for all $v = (w_t, \vec{\varphi}) \in H^0$,

$$B(u, v) = F(v) \quad (3)$$

with appropriate Sobolev spaces H and H^0 , depending on the boundary conditions. Here,

$$B(u, v) = D \int_{\Omega} [(1-\nu) \nabla \vec{\beta} \cdot \nabla \vec{\varphi} + (1+\nu) (\nabla \cdot \vec{\beta}) (\nabla \cdot \vec{\varphi})] d\Omega + \kappa G t \int_{\Omega} (\vec{\beta} - \nabla w) (\vec{\varphi} - \nabla w_t) d\Omega \quad (4)$$

where the first part consists of bending and the second part of the shear, and

$$F(v) = \int_{\Omega} q w_t d\Omega. \quad (5)$$

The finite element approximation u_h will be found in a subspace $S \subset H$ so that (3) holds for every $V \in S^0 \subset H^0$.

We note that the exact solution to (1), (2) with appropriate boundary conditions is characterized by the following effects:

- (1) There exist boundary layers. Boundary layers are components of the solution that vary rapidly and decay exponentially with respect to the distance ρ to the boundary. They are of the form $f(x, y) = \Psi(x, y) \exp(-\alpha \rho / t)$, where $\Psi(x, y)$ is a smooth function and $\alpha > 0$. According to reference 1, $\alpha = \sqrt{12\kappa} = \sqrt{10}$ is the characteristic width of the boundary layer for RM plate bending problems. In particular, the RM plate model shows a strong boundary layer in the vicinity of free and soft simply supported edges, while there is no boundary layer on hard clamped edges.
- (2) There exist point singularities. These are introduced by non-smooth domains as well as by changes in the boundary conditions.
- (3) For $t \rightarrow 0$, the second term in (4) acts as a penalty term enforcing the condition $\nabla w = \vec{\beta}$ (as seen when multiplying the equation by t^{-3}), so that the problem becomes the biharmonic equation. In this case, only point singularities remain on nonsmooth domains or in case of

changing boundary conditions. Due to the penalty term, the RM plate model exhibits a locking effect for $t \rightarrow 0$.

In all our computations, we use an ansatz space of polynomials $\xi^i \eta^j, i, j = 0, \dots, p$ on specifically tailored meshes. The use of polynomials of high order ($p \geq 4$) in itself ensures that the locking phenomenon (3) can be overcome. We use $p+4$ Gauss-Legendre integration points in each direction in all numerical examples. This is over-integration, but with a view to strongly distorted elements and elements with blending function mapping it is reasonable. In none of our computations, there will be any grading of the p . All elements are uniform in p . However, the mesh is not uniform, but specifically tailored to capture the effects noted in (1) and (2) above.

For those parts of the domain where the exact solution is smooth, the most efficient method of approximating it is by using high p on a very coarse mesh.

As demonstrated in references 1, 2, and 3, the boundary layers (1) can be "captured" efficiently by *anisotropic mesh refinement* towards the boundary. It should be noted (and will be seen later on from the numerical examples) that the use of high p on a uniform mesh in itself does not guarantee fast convergence in energy norm or in pointwise results in the presence of boundary layer effects, but may in fact lead to globally oscillating solutions.

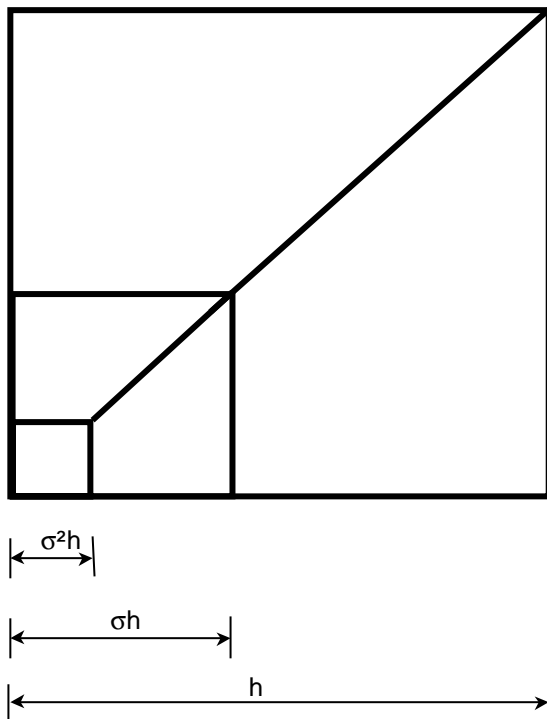


Figure 1: Geometrically graded mesh created by recursive application of a `refine` operation.

In order to "capture" the boundary layer effects (1) properly, a layer of elements of type $(1, O(pt))$ is required where the $O(pt)$ direction is perpendicular to the boundary.

Furthermore, the point singularities noted in (2) above call for geometrically graded meshes with a mesh grading parameter $0 < \sigma < 1$. The point refinement strategy is shown in figure 1. From approximation theory and practical experiences, it is known that a mesh grading factor of around $\sigma = 0.15$ is optimal (slight over-refinement). We refer to the kind of refinement shown in figure 1 as the `refine(double sigma)` procedure henceforth.

In corners, boundary layer and point singularity effects may overlap. In these cases, we introduce geometrically graded sequences of element layers *inside* the boundary layer refinement zone (called thickness-dependent geometric refinement in references 1 and 3). For very thin plates (e.g., $t < \frac{1}{1000}$), when the boundary layer effects are concentrated in a very narrow strip along the boundary, whereas the point singularities are unaffected by the plate thickness in the biharmonic limit, the refinement zone for the point singularities may extend beyond the anisotropic boundary refinement layer. However, as shown in reference 3, even then the loss of efficiency by the "thickness-dependent geometric refinement" approach is small, and plates of such small thickness are outside the range of most practical bending problems.

In summary, we are looking for meshes which meet the following requirements:

- (a) In general, the mesh ought to be *as coarse as possible*. In other words, the geometry of the domain ought to govern element edge sizes.
- (b) On all edges where boundary layer effects occur, we require *one layer* of anisotropic refinement. On hard clamped edges, we do *not* wish to introduce refinements.
- (c) We require the possibility of arbitrarily many layers of geometric refinements in corners as well as points where boundary conditions change. In case of combined edge and point effects, we work with thickness-dependent geometric refinements. We require that elements subject to geometric refinement are not strongly distorted. This is a particularly hard requirement for a fully automatic mesh generator that is at the same time expected to create a very coarse mesh.
- (d) No irregular (hanging) nodes are permitted. Tackling hanging nodes is much more difficult in the p -version than in the classical h -version.

- (e) Before the refinements are introduced, no elements are allowed to contain more than one potentially singular point or two non-adjacent edges with boundary effects.
- (f) The mesh is required to consist exclusively of quadrilaterals. We avoid triangular elements because of a lack of efficient and reliable higher-order quadrature formulas for triangular domains and because the product space of higher-order polynomials is not suitable for triangles.

While the principles guiding mesh generation for the RM plate model are quite clear, it is by no means a trivial task to construct a mesh that fulfills all the criteria noted above, for general geometries and boundary conditions. This holds even for manual mesh design, let alone for *fully automatic mesh generation*. In the following, we outline a strategy for automatic mesh construction adhering to all the mesh design principles noted above.

2. GENERATION OF COARSEST POSSIBLE QUADRILATERAL MESHES

Conventional mesh generators for the h -version of the FEM generally rely on filling any geometry by a large number of small triangles. This kind of an approach is entirely unsuitable for the p -version.

In order to use the p -extension efficiently, we require "coarsest possible" meshes. By such a mesh, we denote a non-uniform regular mesh where the local element size is mainly governed by the edge size of the original domain in the neighborhood of the element. In the p -FEM, requirements on element shapes can be relaxed a bit when focusing on higher-order polynomials.

In the case of multiply connected domains, the edge size may be bounded from above in a natural way by the closest distance between the outer boundary and the boundary of an inner loop (inclusion). The same is true for non-convex domains where the distance between non-adjointing edges of the same loop rather than the edge length may govern the element size.

Every mesh generator for non-uniform meshes needs some background density information $d(x, y)$ for the mesh generation process. From the above description, it becomes clear that, in the case of "coarsest possible meshes", the background density information can be computed as the solution of a boundary value problem. Because the extrema of the density function are expected on the boundaries of the domain, we choose to solve a Dirichlet problem of the Laplacian:

$$\Delta d = 0 \text{ on } \Omega \text{ subject to boundary conditions } d = d_0 \text{ on } \Gamma = \partial\Omega. \quad (6)$$

The function d_0 is determined as the piecewise linear interpolant of pointwise values computed for every corner of the domain by averaging the edge lengths of all edges incident in that corner. However, in those sections of the boundary where some non-incident edge is closer to the boundary than the prescribed density, we replace the prescribed density by the edge-to-edge distance. This is frequently the case when openings are close to the boundary. We refer to problem (6) as the *auxiliary problem* thenceforth.

Any numerical method for solving partial differential equations can be used to approximate the solution of (6). A first-order finite difference scheme in combination with a Gauss-Seidel based solution process might well do. However, we choose a finite element approximation based on a mesh of triangles with piecewise linear ansatz. Figure 2 shows a typical sample mesh used for this process, as well as the contour lines of the resulting mesh density function. The triangle mesh for solving (6) approximately has been generated on the basis of a density function that is constant throughout the domain, and with relaxed distortion criteria.

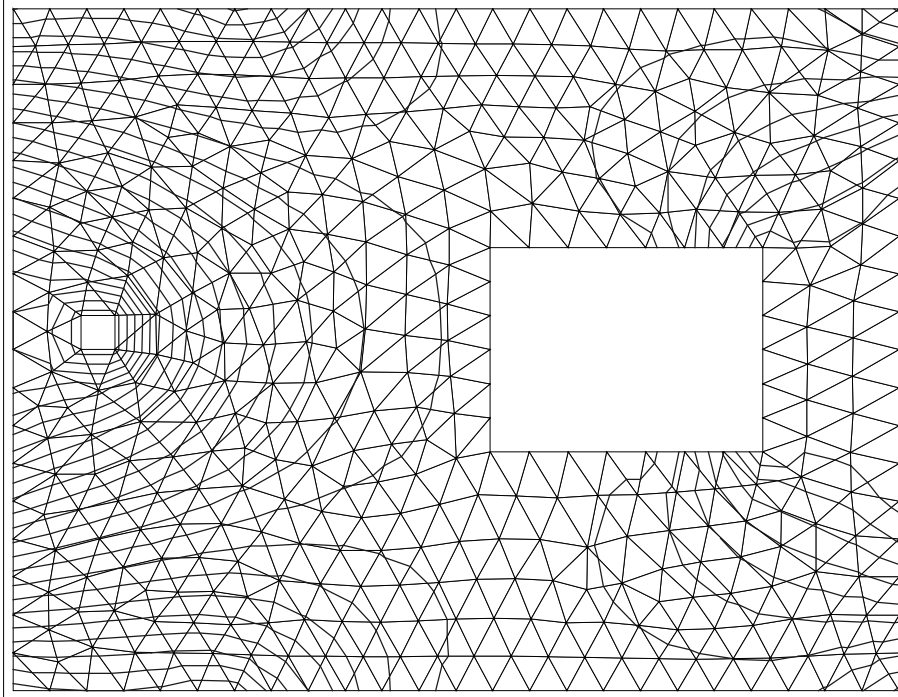


Figure 2: Auxiliary mesh and contour lines of mesh density.

On first sight, our approach may appear somewhat queer as it entails generating a "fine" mesh of triangles first, and even solving a finite element problem just for the sake of coarse mesh generation. The problem size of the auxiliary problem may be of the same order as the original problem. However, we are motivated by the following considerations:

- (1) There is no need to solve the auxiliary problem (6) with anything more than the very crudest accuracy. Therefore, the solution is fast.
- (2) An auxiliary mesh is required anyway, out of the following reason: In our application, we are trying to solve plate bending problems from engineering, where almost inevitably more than one loading and boundary condition case has to be taken into consideration. However, each of these load cases – using specifically tailored meshes – will require an individual finite element mesh. The only thing that remains constant over all load cases is the shape of the domain Ω . In order to perform the superposition and extremum finding for all load cases, a common reference frame is required, independent of finite element meshes and integration points. The mesh associated with the auxiliary problem serves at the same time as the common reference frame. Displacements and stresses are evaluated for each load case in each of the nodes of the auxiliary mesh. Because there are no obvious "superconvergent points" in the p -version, the position of these points inside the finite elements does not matter much. Furthermore, the auxiliary mesh lends itself naturally for graphical result presentation based on linear interpolation in the triangles. In summary, the auxiliary mesh can be utilized for multiple purposes, so that the amount of work spent in its generation is not lost.
- (3) In comparison to the hp -FEM RM plate bending problem, the auxiliary problem is extremely easy and fast. The stiffness matrix can be computed analytically. Of course, the fraction of the total computer time required for creating the auxiliary mesh and solving the auxiliary problem depends strongly on the fineness of the auxiliary mesh. From remark (2), a very fine auxiliary mesh may be required. However, what becomes most costly then is the creation of the fine mesh of triangles, and not so much solving the auxiliary problem on it.
- (4) The mesh generator may exploit not only the approximate density function $d_h(x, y)$, but also its gradient in order to produce a mesh. The gradient information is valuable if there are strongly different edge sizes present in the original geometry of the domain.

The mesh generation technique employed here is the advancing front technique, as described and implemented in reference 4. If the mesh generator fails to generate a mesh (yes, it may happen) with the density information provided, a new density distribution is computed by multiplying the first one by a factor of 0.75. This process is repeated until the mesh generator succeeds.

In a first step, the mesh generator produces a mesh that consists of quadrilaterals and triangles.

In the next step, the mesh is transformed into a purely quadrilateral mesh (requirement (f) from above) by splitting each of the triangles into three quadrilaterals and each quadrilateral into four. This idea has been suggested independently by various authors; we refer to reference 5 here for the purpose. This way, no hanging nodes are produced, so that requirement (d) from above remains valid.

While this "bisection" step effectively halves the element size, which is counter-productive with a view to the "coarsest possible" requirement (a), bisection is nevertheless almost inevitably required in order to fulfill requirement (e). Domains from practical applications typically contain a large number of re-entrant corners close to each other, as well as holes close to the boundary, so that it would be excessively difficult to guarantee requirement (e) without a bisection operation. This is why we even perform the bisection step if no triangles are encountered at all after the first meshing.

After the bisection step, the mesh is subject to a simple Laplace smoothing.

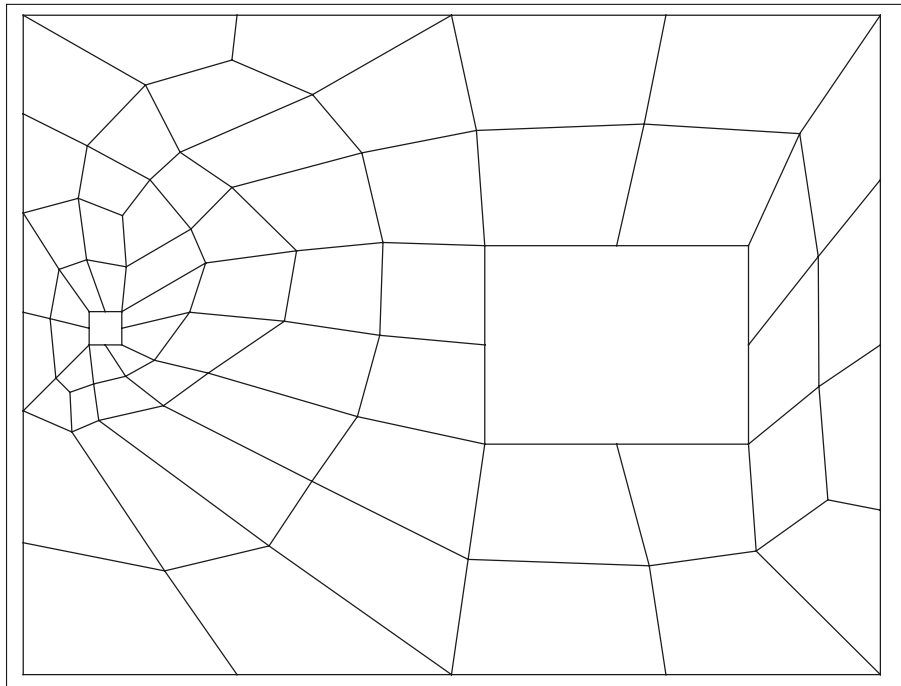


Figure 3: Coarse mesh based on the density data of figure 2.

Figure 3 shows a typical mesh generated by this technique for the domain and density information shown in figure 2. This mesh matches requirements (d) to (f), as well as, *cum grano salis*, requirement (a). It is clear that such a coarse mesh for such a complicated domain cannot consist of "nicely shaped" elements, but, as noted above, requirements on distortion can be greatly relaxed when using high-order polynomial ansatz functions.

3. ANISOTROPIC EDGE REFINEMENT

The next question is how to create meshes with proper edge refinements, as required in (b) above. Simultaneously, we stay aware of requirements (c) (point refinement) and (d) (no irregular nodes).

We have explored the following two approaches:

- (1) Generate the boundary refinements first, then triangulate the interior of the domain.
- (2) Create a "coarsest possible mesh" first, then introduce the boundary refinements "after the fact".

Both approaches will be briefly discussed here.

Figure 4 shows a typical mesh created from the first idea. The domain is the same as in figures 2 and 3. Boundary conditions are hard clamped support on the outer boundary, and all edges of the two holes are free edges. We introduce the boundary refinements prior to generating the interior mesh. When comparing to figure 3, some problems become evident. In order to be able to insert thickness-dependent geometric refinements in the corners without introducing either hanging nodes or extremely distorted elements, we have to put square elements in each re-entrant corner with boundary layer effects. The mesh generator has obvious problems in joining these small features produced by the edge layers to the coarse mesh elsewhere, and the mesh generation scheme will frequently fail, i.e. try again with a globally smaller element size.

Naturally, the mesh bisection for the triangle-to-quad transformation operates also on the boundary refinements and on the squares in the corners, thus producing in effect two layers of edge elements. Especially with the small hole, it is obvious from figure 4 that it is often difficult to put all required features on boundaries and corners. In total, the mesh displayed in figure 4 contains 408 elements.

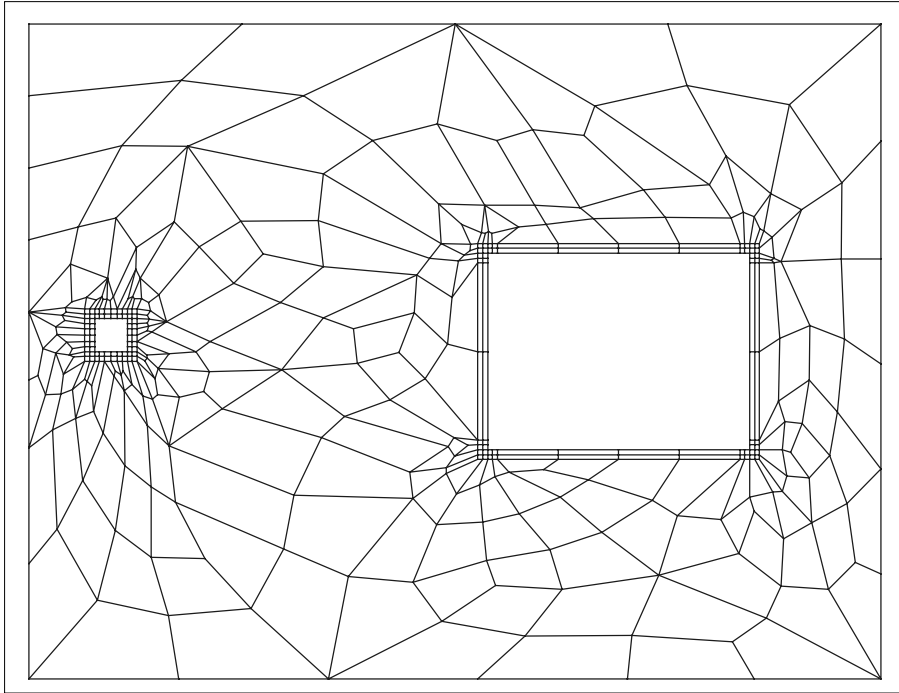


Figure 4: Mesh with boundary refinements created *before* meshing the interior of the domain.

In summary, this approach will frequently fail and will not produce meshes that are *coarse enough*.

Therefore, a second approach, namely after-the-fact refinement, has been examined closely.

In principle, it is easy to introduce the anisotropic refinement "after the fact", as shown in figure 5. From now on, we refer to the mesh refinement scheme shown in figure 5 as the `split` operation on the finite element edges emanating from the boundary of the domain, followed by a `cut` method. The `split` operation is applied to all finite element *edges* emanating from domain edges that call for boundary refinement. This produces 6-noded polygons, which can be easily `cut` into two quadrilaterals subsequently.

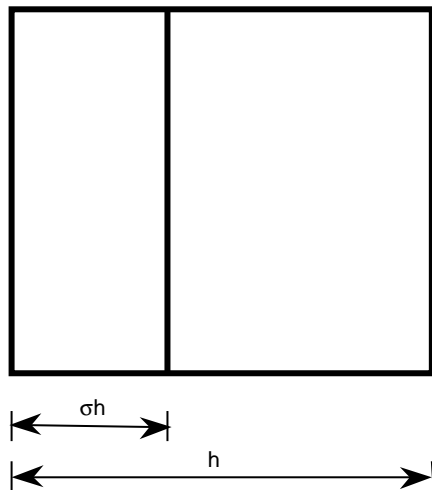


Figure 5: Anisotropic mesh refinement on the boundary created by `split` and `cut` operations.

However, a problem occurs in corners. Any corner element has two adjoining edges, both of which receive a `split` refinement. In this case, we cannot apply `cut` (which would produce a triangle and a pentagon), but we need a special scheme to "get around the corner".

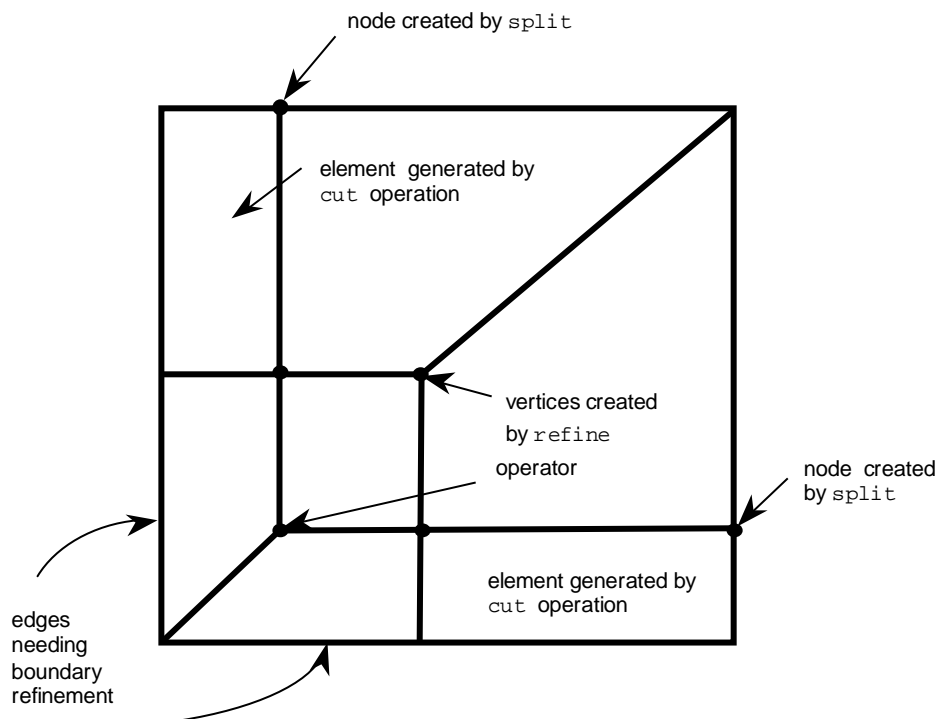


Figure 6: Solution to the corner problem associated with the anisotropic boundary refinement.

The idea how to overcome this problem is simple, but efficient, as shown in figure 6. Before the `split` operations, we perform a `refine` operation towards the corner vertex. Although this operation *looks* like the geometric corner refinement, it is not one, but serves the sole purpose of

getting the boundary refinements around the corner. Therefore, the refinement factor σ may be anything between 0 and 1. In addition, we would like to have it such that, after introducing the boundary refinements, the resulting elements are not too distorted. At the same time, we would like to have the new rectangular element in the corner to be of about twice the $O(pt)$ size of the boundary refinements. We ignore the p -dependency as in references 1 and 3 and use a fixed width of the boundary refinement, independent of p , by substituting $p_{\max} = 8$. σ will be chosen accordingly.

Therefore, we extend the `refine` function by limiting values $0 < \sigma_{\min} \leq \sigma \leq \sigma_{\max} < 1$. We use $\sigma_{\min} = 0.0001$ and $\sigma_{\max} = \frac{2}{3}$, which seems to be a reasonable choice. Our numerical experiments show that elements with an aspect ratio of 1/10000 do not cause numerical instabilities, provided they are sufficiently close to a rectangular shape.

In the next step, we introduce the refinement in the two skew elements by applying the `split` operator on the two new edges emanating from the boundary. In this case, the refinement factor is chosen such as to produce an element of width $O(p_{\max}t)$, i.e., reasonably close to 0.5. Like the `refine` operator, the `split` operator is extended to include an upper and lower bound on the refinement factor σ . Once again, we impose $\sigma_{\max} = \frac{2}{3}$. This means over-refinement for relatively thick plates. For extremely thin plates, our lower bound on σ will cause under-refinement. However, our numerical examples show that the results are quite insensitive to the width of the anisotropic boundary refinement zone, and the effects introduced by bounding the refinement parameter are even favourable.

We can now apply `cut` to the two skew elements. Finally, we close the refinement layer by inserting an *inverted refine* layer in the corner rectangle (now a hexagon). In this case, the refinement factor is given by $1 - \sigma$, where σ is average of the actual factor chosen in the `split` operation of the two `split` edges (i.e, the average of two values reasonably close to 0.5).

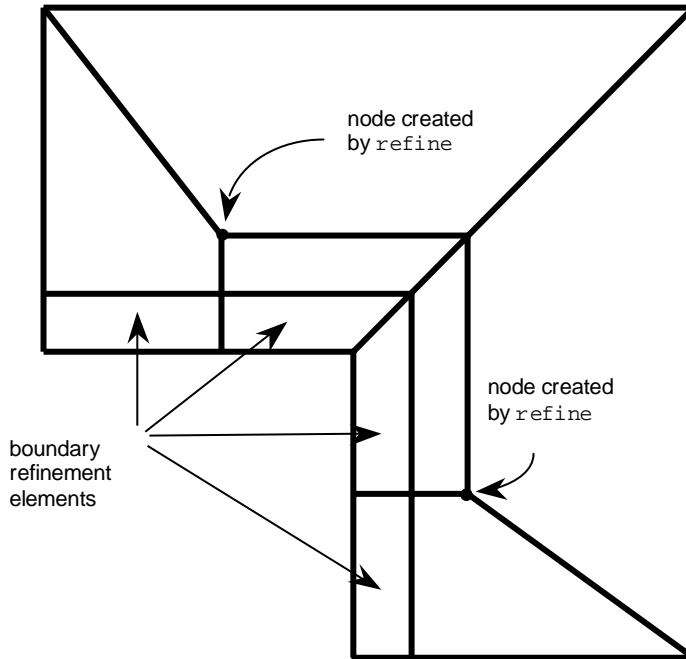


Figure 7: Re-entrant corner. First case.

This description is valid for a non-re-entrant corner. However, re-entrant corners can be handled much in the same spirit. The case of figure 7 is almost the same as the one in figure 6. Now, the first `refine` operation serves the purpose of creating a well-shaped boundary refinement element in the corner which is suitable for subsequent geometric refinement. However, we do not need a second `refine` operation in order to get the corner closure, but a simple `cut` operation is sufficient.

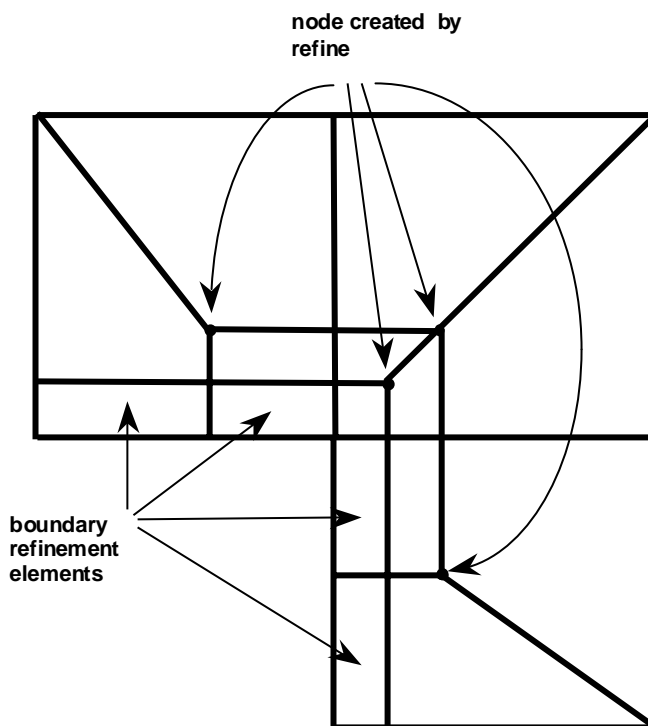


Figure 8: Re-entrant corner. Second case.

Even the case in figure 8, which seems different, can be handled easily: Now, the closure by the `refine` operation is applied to the corner node rather than the new node, and once again the boundary refinement gets "around the corner".

A closer inspection reveals that, in fact, both cases (figs. 6 and 8) are algorithmically the *same*: The question is simply to which vertex the closing `refine` operation ought to be applied. The required vertex is readily identified to be the node between the two new nodes generated by the `split` operation. Therefore, it is simply necessary to mark the new nodes, and it is then an easy task to find the `refine` vertex by checking adjacency relations.

We note that all the elements directly adjacent to the corner node in figures 6 through 8 may be subject to a further geometric refinement in the next step. Note that these elements are all well shaped, generally not much exceeding an aspect ratio of 2/1. The worst case is the case of figure 7, where the corner angle might become sharper than in our drawing.

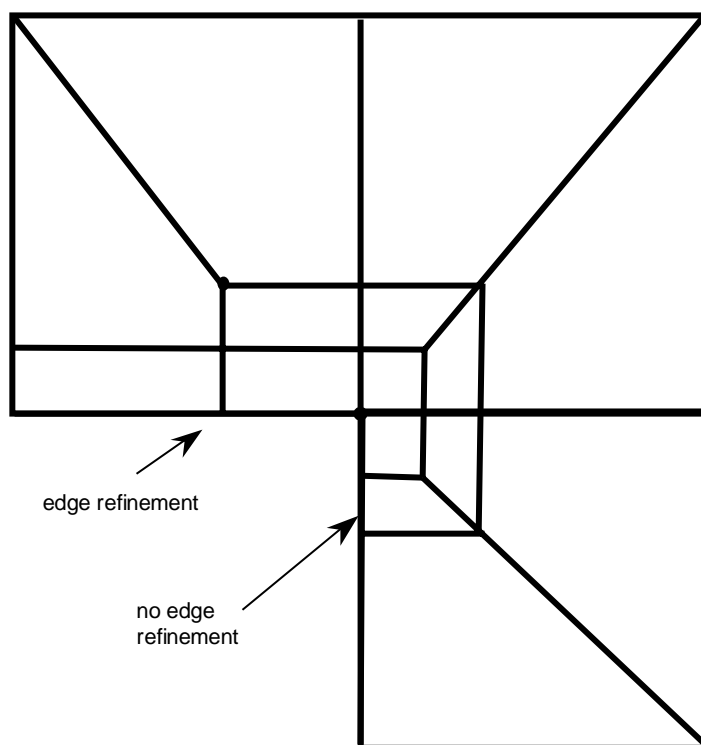


Figure 9: Re-entrant corner with boundary refinement on one side only.

Finally, we have to deal with the case of a corner that joins two domain edges, only one of which requires a boundary refinement. Figure 9 displays an example of this situation and our meshing

solution. In this case, all element edges emanating from the domain edges that require edge refinement are `split` accordingly, and once again the closure can be obtained exclusively by the `refine` and `cut` operations. Furthermore, this strategy produces a situation that is once again ideally suited for inserting geometric refinement layers in the next step.

The same considerations as explained above for figure 9 also hold for the case of points on the boundary of the domain where the type of prescribed boundary condition changes, although these points need not be actual corner points. Also, the practically relevant case of multiple subdomains (domains which include vertices where more than two edges are incident) is also readily included in our approach.

In summary, we first apply the `refine` operation to *all* nodes on the boundary of the domain that are either corners, points of changing boundary conditions, or points where multiple subdomains meet. In a second step, we apply the `split` operation to all finite element edges emanating from domain boundaries that require edge refinement. Finally, we close the resulting hexagons by either `cut` or another `refine`. In summary, one needs to implement only three topological/geometrical operators in order to cover all possible cases. Moreover, the `refine` operator also solves the next task, the geometric refinement.

Figure 10 shows once again the domain familiar from figures 2-4. Now, we apply the after-the-fact boundary refinement on the basis of the mesh shown in figure 3. The mesh has now 159 elements, i.e. little more than one third of the number of elements created by the "boundary mesh first" approach in figure 4.

The upper bound σ_{\max} which we have put on the refinement operators comes into effect on the small hole, which has a diameter of only $5t$. Although the mesh around this small hole looks somewhat unusual, the elements are in fact quite well-shaped.

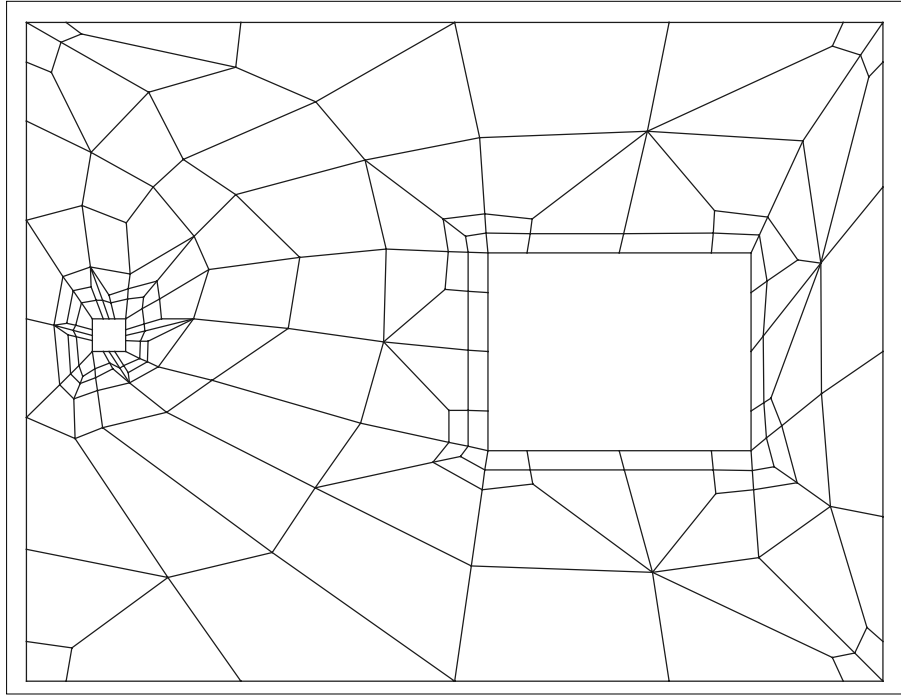


Figure 10: Coarse mesh with boundary refinements introduced *a posteriori*.

4. THICKNESS-DEPENDENT GEOMETRIC REFINEMENT

It has already been said that our boundary refinement algorithm produces ideal starting situations for a subsequent thickness-dependent geometric mesh refinement. We can be quite sure that all elements adjacent to singular points are well-shaped. These elements have either been created by the original meshing algorithm from section 2, or by the boundary refinement procedure from section 3. The operator `refine` required has already been introduced in section 3. For all potentially singular points, this operator is now applied repeatedly (usually, in practice, once or twice; all our practical numerical examples are based on 2 recursive geometric refinements, but, for practical purposes, one layer would often suffice for obtaining an error in energy norm of around 1%).

Figure 11 displays the mesh layout produced by our algorithm after all these steps. The problem is once again the same as the one already presented in figures 2-4 and 10. There are two layers of elements in geometric progression in each of the re-entrant corners. Now, the mesh consists of 243 elements in total. Figure 12 displays the results of a computation with this mesh. The plate is clamped on all outer boundaries, and all the holes have free edges. The loading is uniform pressure. Poisson's ratio is $\nu = 0.2$, and the thickness-to-span ratio of the plate is $t/L = 1/100$. The convergence curve displayed is based on an extrapolated limiting value of the strain energy. It is obvious that the p -extension on the fully automatically generated mesh performs very efficiently. With something around 10000 unknowns, an accuracy of 1% in the energy norm can be obtained.

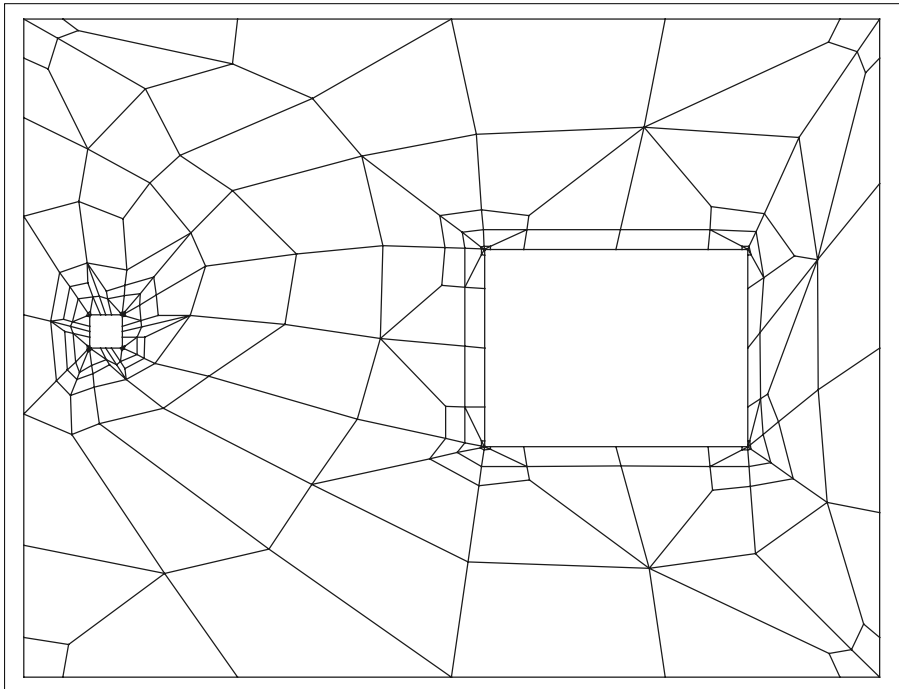


Figure 11: Mesh from figure 10 after geometric refinement in re-entrant corners.

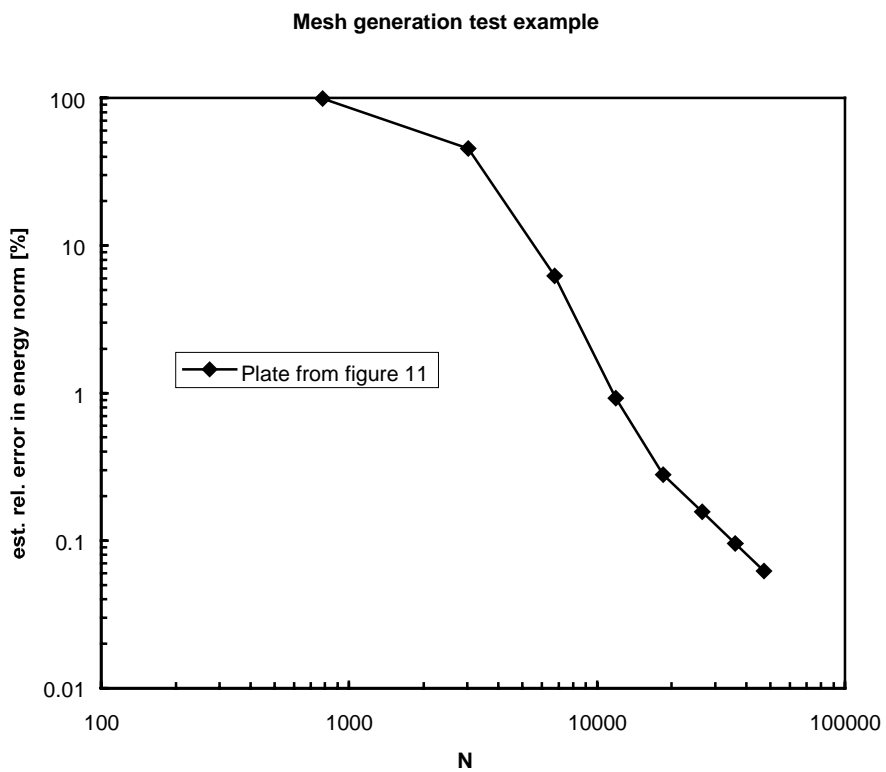


Figure 12: Convergence of the error in energy norm for the mesh from figure 11.

5. NUMERICAL EXAMPLES

In this section, we report results obtained by the hp finite element RM plate code *Plate32* developed by the author for research purposes, but also for practical applications for *HOCHTIEF* construction company, Frankfurt, Germany.

In practical engineering applications from civil engineering, common thickness to span ratios are in a range of 1/10 to 1/100 in concrete plates and perhaps up to 1/1000 in steel plates.

In our first numerical example, we explore the effect of the width of the boundary refinement zone on the global accuracy in the energy norm.

To this end, we analyze a rectangular plate of proportions 0.7/1.0 subject to constant load and soft simple support on all sides. Poisson's ratio is $\nu = 0.2$. We analyze this plate for the thickness to span ratios 1/50, 1/500 and 1/5000. Because an exact solution of the RM plate problem is not available for this case, we use a series of overkill solutions and Richardson extrapolation to estimate the limiting value of the strain energy.

We use meshes produced by our fully automatical mesh generator. We use boundary refinements, but no geometric point refinements.

Figure 13 displays the estimated relative error in energy norm as a function of the width of the boundary layer elements for each of the three thickness to span ratios. All these results are for uniform $p=8$. It is clearly visible that the width of the refinement zone has no strong influence on the accuracy of the results, especially for thin plates (Note that all the results are in a range of 0.04 to 0.6 % relative error in energy norm). Therefore, we feel justified to use boundary refinement elements corresponding to $3t$ in our other examples, independent of p .

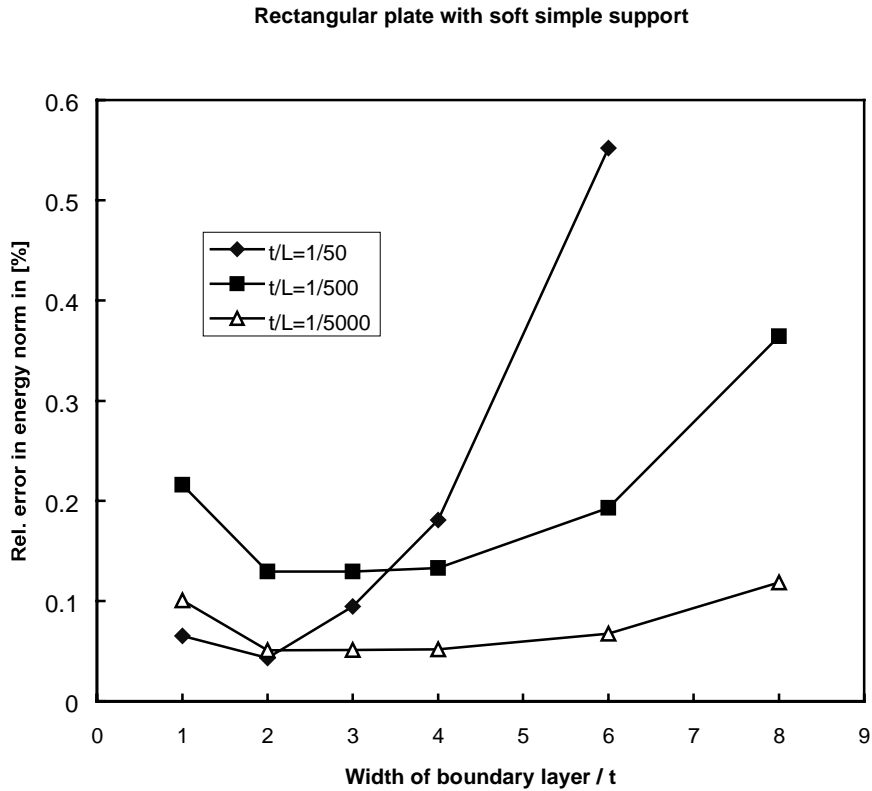


Figure 13: Influence of the width of the boundary refinement on the error in energy norm at $p=8$. Rectangular plate with soft simple support under uniform pressure.

Figure 14 corresponds to a very similar example, a soft supported plate under uniform pressure, however, with proportions $0.8/1.0$ and $\nu=0$. In this figure, we compare results obtained with a uniform mesh (2×2 elements) and results obtained with a mesh that includes a boundary refinement zone for a thickness to span ratio of $1/50$. Our fully automatically generated mesh is displayed in figure 15. An analytical solution for Kirchhoff plates is available for this problem, however, pointwise accuracy will be discussed elsewhere.

It is evident from the global convergence curve in figure 14 that the boundary refinement is definitely required to achieve sufficient engineering accuracy.

While these examples display only the influence of the boundary layer effect, we have also studied the example given in reference 3 for a combination of edge and corner effects. Figure 16 shows our fully automatically generated mesh for a thickness-to-span ratio of $1/100$. Prior to introducing the thickness-dependent geometric refinement, this mesh consists of 48 elements. The corresponding mesh in

reference 3, manually created, has 19 elements for that. We use the mesh topology shown also for a thickness-to-span ratio of 1/1000.

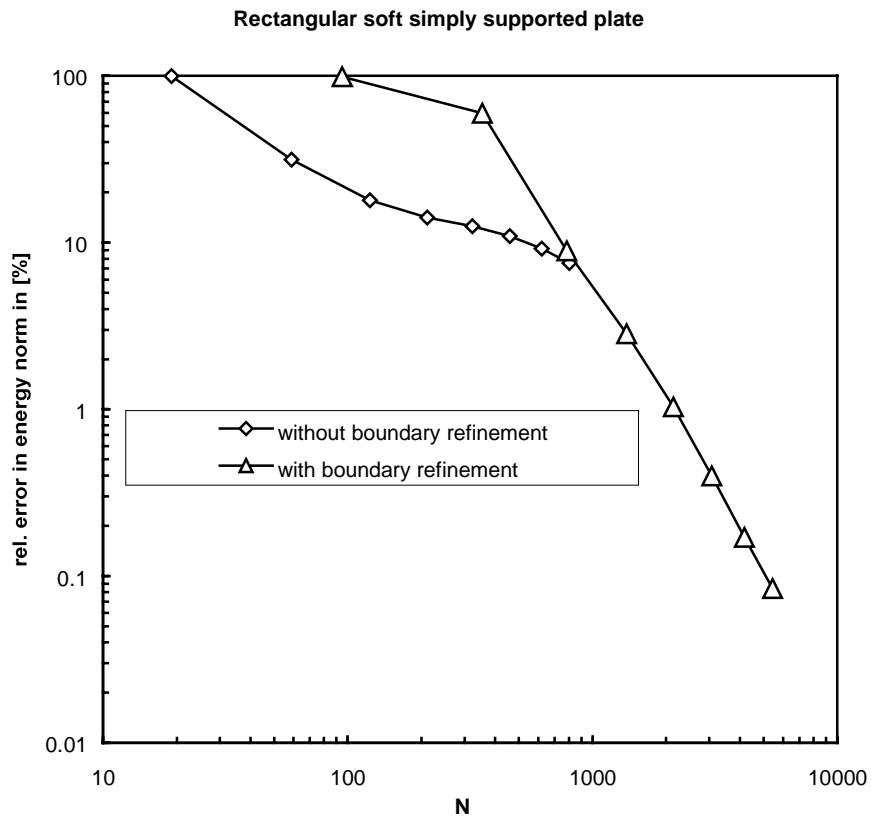


Figure 14: Effect of the boundary refinement on the error in energy norm.

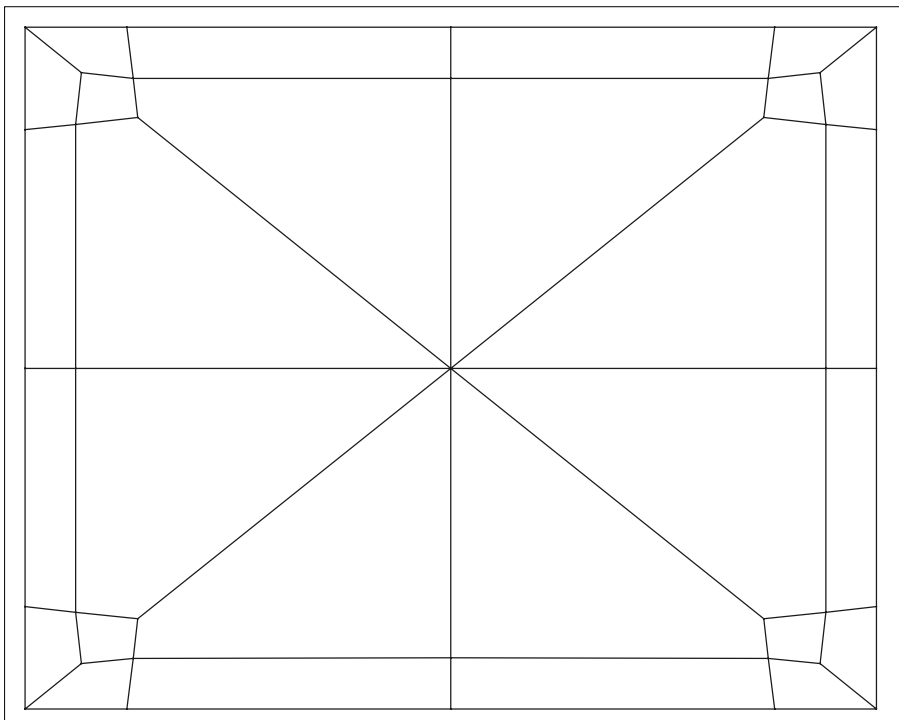


Figure 15: Mesh used in figure 14.

For very thin plates, as noted in references 1 and 3, the thickness-dependent geometric refinement becomes less efficient because the plate model approaches the Kirchhoff (biharmonic) model, where corner singularities exist which are independent of the thickness. In order to capture these properly, a thickness-independent geometric refinement would be required, which is not feasible with the automatic mesh generation approach presented here. However, it has already been pointed out by reference 3 that the loss of efficiency is not very marked, and we may add the consideration that plates in a thickness range of below or around $1/1000$ are practically not relevant.

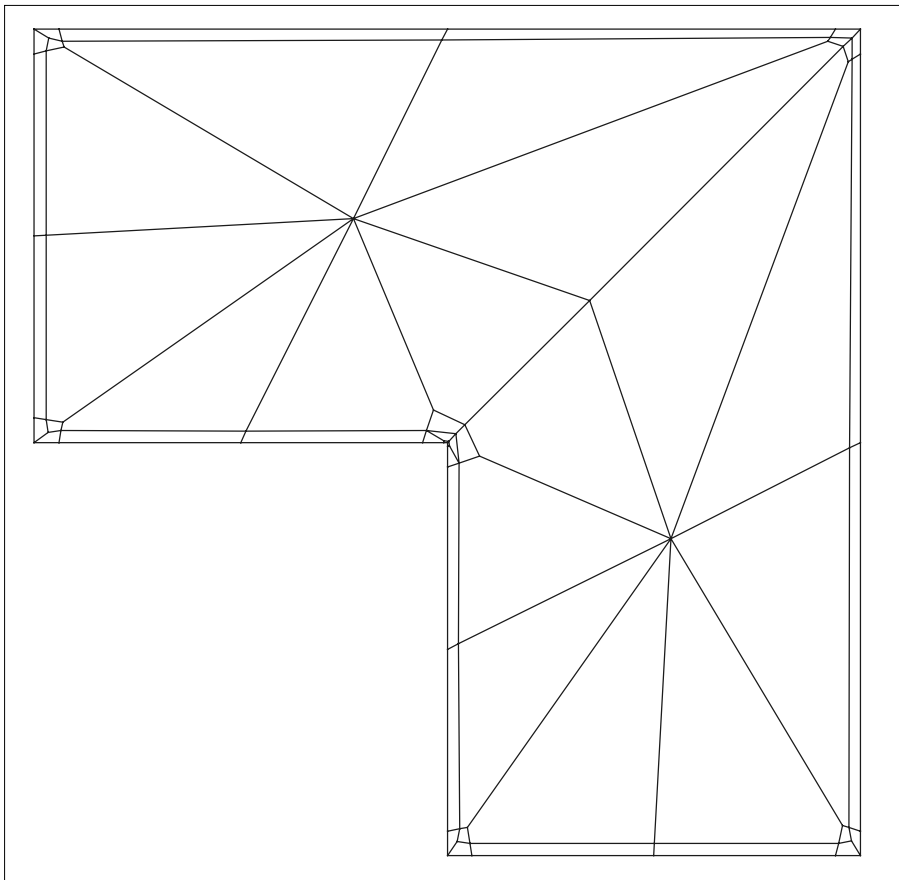


Figure 16: Mesh for problem with combined edge and point singularity effects.

Nevertheless, there exists a remedy for thin plates. As indicated in figure 13, the influence of the width of the boundary layer refinement becomes less obvious for very thin plates. Therefore, we choose to lose a little bit on the boundary layer approximation by using a mesh with a boundary layer element width of $10 \cdot t$. At the same time, we gain in the approximation of the point singularity. Figure 17 shows the numerical results for this approach. We display the convergence of the error in energy norm for various refinement strategies. We try various layers of geometric refinement towards the re-entrant corner, as well as some meshes with combined boundary layer and thickness-dependent geometric

refinements. As in figure 14, it becomes clear that engineering accuracy can only be obtained when using both boundary and point refinements. This remark is also underlined by the numerical results for moderately thin plates, not reported here for space reasons.

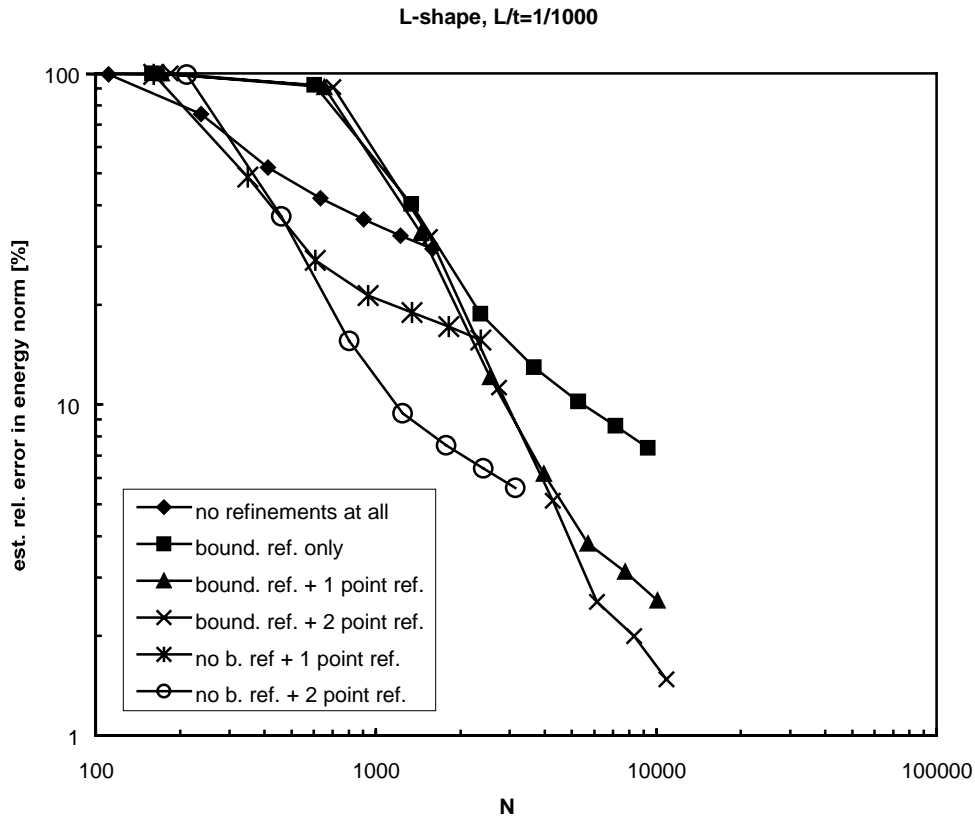


Figure 17: Convergence of the estimated relative error in energy norm of the L-shaped plate for a thickness-to-span ratio of $1/1000$. The width of the boundary refinement elements has been chosen to be equal to $10 t$.

The final example is to show that automatic mesh generation with a reasonable number of elements for *hp*-type finite element approximation of RM plate bending problems is possible not just for academic cases, but also for practical applications.

Figure 18 shows the mesh constructed for a moderately thick plate with various openings and many corners and other singular points, subject to constant load. The mesh has free boundary conditions on all the openings, entailing boundary mesh refinements there. Furthermore, four edges on the lower side of the plate have soft simple support, and one edge on the upper side is also free. The mesh shows our boundary refinement layer on all these edges, and no layers on the rest of the edges, which are hard clamped. Of course, there exists a large number of point singularities, introduced by the re-entrant

corners and by the changes in the boundary conditions. All of these have been covered by two layers of thickness-dependent refinements each.

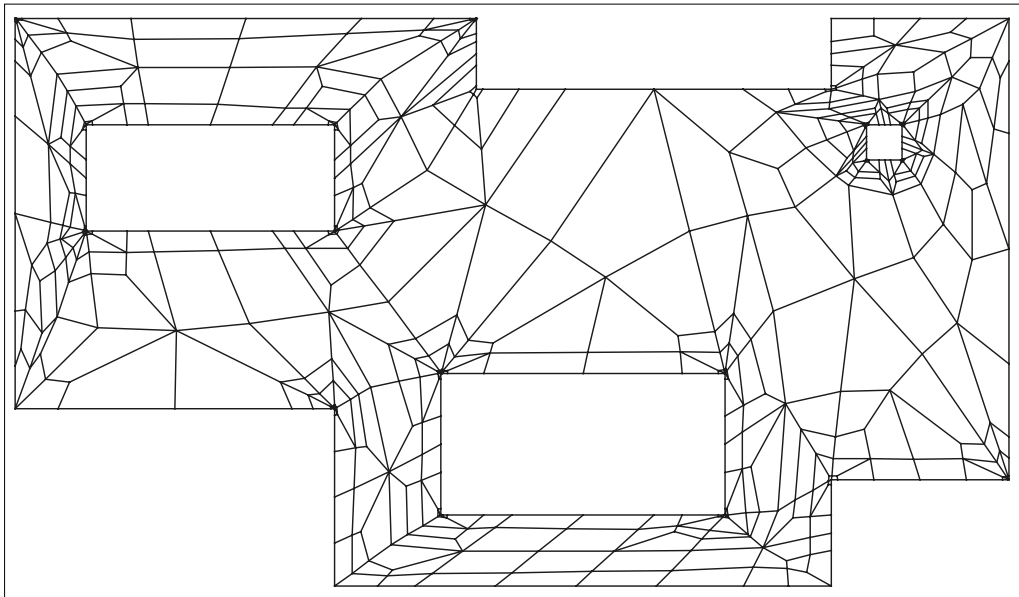


Figure 18: Automatically generated mesh for a practical example.

The convergence of the estimated error in energy norm is displayed in figure 19. This figure is based on an extrapolated "exact" value of the strain energy. On a PentiumPro 200 MHz PC with 256 MB of memory, the total computation time of this example for $p=8$ (101605 unknowns, 525 elements) was 781 seconds. The solver took about 75% of the total time.

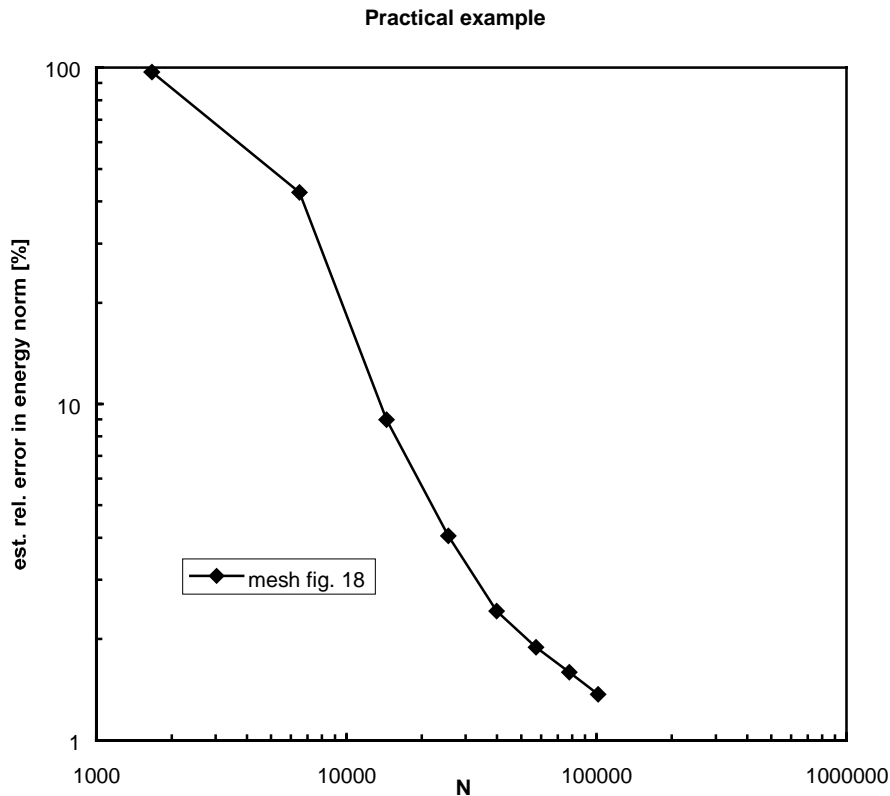


Figure 19: Convergence of the estimated relative error in energy norm for the practical example displayed in figure 18.

CONCLUSIONS

We have presented a method for fully automatic generation of meshed that are specifically tailored to capture all relevant effects of RM plate bending theory. We have outlined a general approach to *coarse mesh* creation, and suggested a way of combining edge and point refinements for general geometrical situations. We use only three simple topological operations for the refinement process. We have provided experimental numerical evidence that p -extension on these meshes performs very efficiently, so that reliable solutions even for complicated practical problems can be obtained with limited resources in computer time and storage.

ACKNOWLEDGEMENTS

The author would like to thank Norbert Rehle⁴ for providing the advancing front algorithm used in our mesh generator and the extensions required to create the mesh displayed in figure 4. Also, many helpful discussions are acknowledged.

REFERENCES

1. C. Schwab, M. Suri and C. Xenophontos, 'The hp finite element method for problems in mechanics with boundary layers', *Comput. Meth. Appl. Mech. Eng.* **57**, 311-334 (1998).
2. J. M. Melenk, 'On robust exponential convergence of hp finite element methods for problems with boundary layers', Research Report, Seminar für Angewandte Mathematik, ETH Zürich, (1996).
3. C. A. Xenophontos, 'Finite element computations for the Reissner-Mindlin plate model', *Comm. Numer. Meth. Eng.* **14**, 1119-1131 (1998).
4. N. Rehle, *Adaptive Finite Element Verfahren bei der Analyse von Flächentragwerken*, Ph. D. thesis, Universität Stuttgart, 1995.
5. E. Rank, M. Schweingruber and M. Sommer, 'Adaptive mesh generation and transformation of triangular to quadrilateral meshes', *Comm. Appl. Numer. Meth.* **9**, 121-129 (1992).
6. B. A. Szabo and I. Babuska, *Finite Element Analysis*, John Wiley & Sons, New York, 1991.